Low-temperature anharmonicity and the thermal conductivity of cesium iodide

Bin Wei,[1] Xiaoxia Yu,[1] Chao Yang,[1] Xin Rao,[2] Xueyun Wang,[1] Songxue Chi,[3] Xuefeng Sun,[2,4,5] and Jiawang Hong[1,*]

[1]*School of Aerospace Engineering, Beijing Institute of Technology, Beijing 100081, China*

[2]*Department of Physics, Hefei National Laboratory for Physical Sciences at Microscale, and Key Laboratory of Strongly-Coupled Quantum Matter Physics (CAS), University of Science and Technology of China, Hefei, Anhui 230026, China*

[3]*Neutron Scattering Division, Oak Ridge National Laboratory, Oak Ridge, Tennessee 37831, USA*

[4]*Institute of Physical Science and Information Technology, Anhui University, Hefei, Anhui 230601, People's Republic of China*

[5]*Collaborative Innovation Center of Advanced Microstructures, Nanjing University, Nanjing, Jiangsu 210093, People's Republic of China*

Cesium halide has a simple cubic crystal structure and hosts low thermal conductivity, but its microscopic mechanism has not been fully understood. In the present work, we took cesium iodide (CsI) single crystal as an example, to investigate the lattice dynamics and thermal conductivity by performing inelastic neutron scattering (INS), heat transport measurements, and first-principles calculations. The temperature dependent phonon dispersions of CsI were obtained from INS and the low temperature anharmonicity of transverse optic (*o*) and transverse acoustic (*a*) phonon modes in CsI was observed. By performing the thermal conductivity measurement and first-principles calculations, it is shown that the low thermal conductivity of CsI originates from the combined effect of the small phonon group velocities and the large phonon scattering rates, which is dominated by the (*a*, *a*, *a*) and (*a*, *a*, *o*) phonon scattering processes. This work highlights the importance of phonon anharmonicity in lattice dynamics, which sheds light on the design of materials with low thermal conductivity.

I. INTRODUCTION

Cesium halides (e.g., CsCl, CsBr, CsI) possess fascinating electro-optic, electro-mechanic, and large dielectric constants properties [1–3]. These outstanding physical properties are closely related to the thermal transport properties, particularly lattice thermal conductivity (κ) [4]. Cesium halides exhibit low κ, roughly 1 W/mK at room temperature [5,6]. Generally, the low thermal conductivity often appears in materials with inherent soft bonds [7], disordered states [8], and complex crystal structures etc. [9,10]. However, for cesium halides, which are crystallized into simple cubic structures ($Pm\bar{3}m$), none of the above mentioned features are involved. To clarify the origin of the low thermal conductivity in cesium halides, numerous studies have been devoted and several explanations have been proposed [11–14]. However, its microscopic mechanism, such as phonon-phonon scattering and phonon anharmonicity, is still little known for simple structure cesium halides [15–18].

Anharmonicity, defined as the nonlinear relationship between the force and atomic displacement, is closely related to the negative thermal expansion, lattice thermal conductivity, multiferroicity and high-T_c superconductivity, etc. [19–23]. Recently, phonon anharmonicity has received intensive attention and it has been revealed to have a significant contribution to the low thermal conductivity of simple-structured compounds, such as PbTe [24], SnTe [25], SnSe, etc. [21]. As

is well known, phonon anharmonicity usually becomes more significant at high temperature due to the large amplitude of the atomic vibration. Surprisingly, low temperature anharmonicity was recently discovered in CsCl by high-resolution x-ray diffraction [26]. It will be interesting to investigate whether this low temperature anharmonicity also exists in other cesium halides and how it contributes to the low thermal conductivity of such simple cubic materials.

In this work, we selected cesium iodide (CsI) to investigate the low temperature anharmonicity and the phonon transport mechanism of low thermal conductivity of cesium halides due to its relatively easy synthesis and high stability in air. By combining the inelastic neutron scattering (INS), heat transport measurements and first-principles calculations, we obtained the temperature dependent phonon dispersions and observed the low temperature phonon anharmonicity of the transverse acoustic (TA) and transverse optic (TO) phonon modes in CsI, which is also confirmed from the large mode Grüneisen parameters. This is an interesting and unusual phenomenon because the anharmonicity usually becomes more significant at high temperature due to the larger amplitude of the atomic vibration than at low temperature. Our results show that this large phonon anharmonicity, together with small group velocities and large (*a*, *a*, *a*) and (*a*, *a*, *o*) phonon-phonon scattering processes, leads to the low thermal conductivity in the simple cubic CsI. The present results offer a microscopic insight on the phonon anharmonic effect and thermal transport mechanism in CsI, which could be extended to other cesium halides materials.

*Corresponding author: hongjw@bit.edu.cn

184301-1
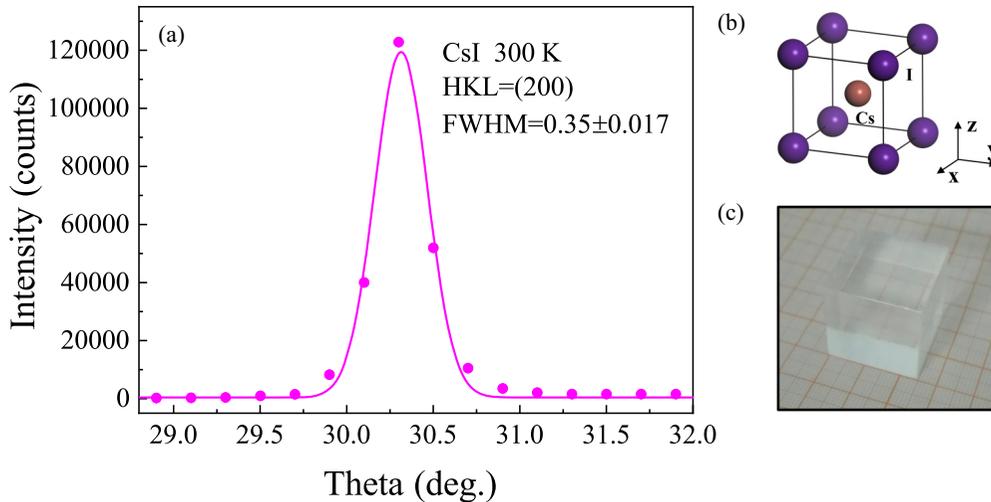
FIG. 1. (a) Rocking curve of CsI single crystal for Bragg showing the high quality of the crystal. (b) The simple cubic crystal structure of CsI. (c) The single crystal sample of CsI ($20 \times 20 \times 20$ mm cubic).

II. EXPERIMENTS AND CALCULATIONS

High quality CsI single crystal [$20 \times 20 \times 20$ mm cubic, the sample information is shown in Fig. 1] grown by the Bridgman technique [27], was used for the INS measurement with the [001] vertical axis. It was performed on the triple-axis HB-3 spectrometer from the High Flux Isotope Reactor at Oak Ridge National Laboratory, by using the PG002 monochromator and analyzer, with a constant final energy $E_f = 14.7$ meV, and collimation settings of 48-40-40-90. The instrument resolution function was calculated in the RESLIB code [28] by inputting the HB3 spectrometer setting for CsI measurement. Subsequently, the phonon energy and linewidths were extracted by computing the convolution of the resolution with a damped harmonic oscillator (DHO) function using the PAN/DAVE software packages. The DHO function is defined as [29]

$$S(\omega) = [1 + n(\omega)] \frac{1}{\pi M} \frac{\gamma \omega}{(\omega - \omega_0)^2 + (\gamma \omega)^2} \quad (1)$$

where M is the atomic mass, ω_0 is the bare phonon energy in the absence of damping forces, and 2γ is a damping factor that describes the phonon scattering rates. $n(\omega) = (e^{\hbar\omega/kBT} - 1)^{-1}$ is the Bose occupation.

The sample for thermal conductivity measurement was cut precisely along the crystallographic axes with dimension of $4 \times 1 \times 0.5$ mm, with [100] axis (a axis) along the length direction. The thermal conductivity along the a axis (κ_a) was measured by using a "one heater, two thermometers" technique in a ^{4}He pulse-tube refrigerator from 18 to 300 K [30].

All first-principles calculations were performed on the basis of the density functional theory (DFT) as implemented in the Vienna *Ab Initio* Simulation Package (VASP) [31]. The exchange-correlation energy was computed using the local-density approximation (LDA) functional and the Ultrasoft pseudopotential was used ($6s^1 5p^6$ for Cs and $5s^2 5p^5$ for I). For plane wave expansion in reciprocal space, we used 500 eV as the kinetic energy cutoff value. The k mesh employed in

the first irreducible Brillouin zone was $8 \times 8 \times 8$, generated by a Γ-centered method. The convergence criteria for total energy was set to 1×10^{-6} eV and that for atomic force was 10^{-3} eV/Å. The structure was fully relaxed and the lattice constant is 4.530 Å, which is slightly smaller than the experimental value (4.533 Å obtained from HB3).

The PHONOPY code [32] was used to calculate the phonon dispersion of CsI at the level of harmonic approximation. In the approach, the second-order interatomic force constants (IFCs) were computed by the finite difference method in a $4 \times 4 \times 4$ supercell of CsI. The Γ-centered k mesh used in all calculations was $2 \times 2 \times 2$. In order to describe the three-phonon scattering processes, the anharmonic third-order atomic force constants must be evaluated for the crystal structures, and the third nearest neighbors were included. Finally, the phonon transport properties were obtained by solving the phonon Boltzmann transport equation (BTE) as implemented in the ShengBTE package [33].

III. RESULTS AND DISCUSSION

A. Phonon dispersions and low temperature anharmonicity

Figure 2 shows the phonon dispersions of CsI at 20, 150, and 300 K from INS along Γ-X and Γ-M directions. The phonon dispersions and the density of states (DOS) from the first-principles calculations (at 0 K) are presented as well. It can be seen that the calculations agree well with our INS measurements for acoustic modes. However, calculations overestimate the high energy optical modes, due to the underestimates of the lattice constant of the LDA exchange-correlation function. For the measured phonons, the LA branch crosses with the TO branch along Γ-X, while it is avoids crossing with TO along Γ-M. The phonon energies soften with temperature increasing from 20 to 300 K. From the partial phonon DOS, it can be seen that the Cs atoms dominate the vibrations in the low energy level due to its heavy mass, while I atoms contribute more to the high energy optic phonons. Only one TA and TO mode exhibits in the spectra along Γ-X due to the degeneration of high crystal structure symmetry. It can also
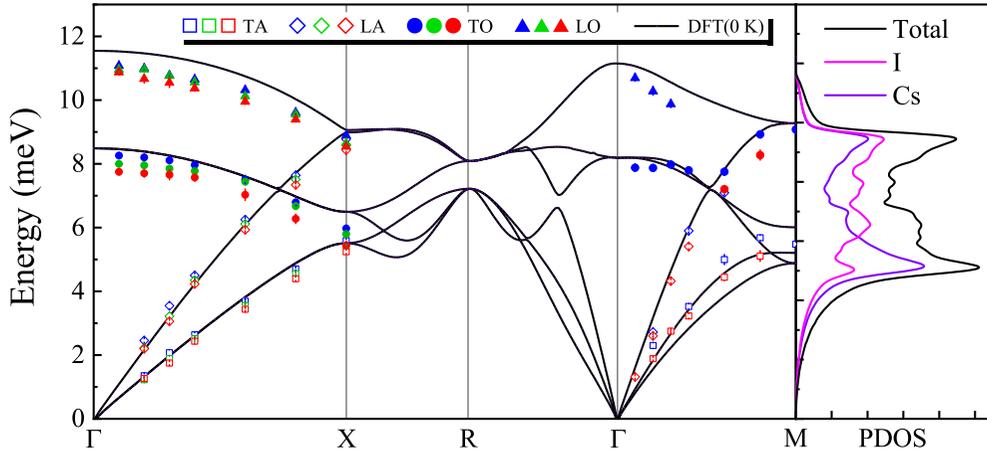
FIG. 2. Phonon dispersions and phonon DOS of CsI. The symbols are from the INS measurement at 20 (blue), 150 (green), and 300 K (red), the curves are from the first-principles calculations. The error bars are from fitting uncertainties and are indicated by verticals. They are all comparable to or smaller than the data point symbols (the maximum value of the error bars is $\pm$ 0.18 meV).

be noted that there is no phonon gap between the optic modes and the acoustic modes, which indicates the possible existence of large phonon scattering space and hence the low thermal lattice conductivity (discussed in detail below).

The low temperature anharmonic effect in cesium chloride (CsCl) was reported recently, as reflected by the unusual displacement of Cs atoms [26]. Alternatively, the anharmonicity can also be shown in the phonon spectra by the large phonon linewidth and the asymmetric line shapes, etc. [34–36]. Figure 3(a) shows the line shapes at $\mathbf{Q} = (2.7, 1, 0)$ with temperature ranging from 20 to 300 K, from which the TA and LA phonon modes clearly shift to lower energies when the temperature increases. The phonon linewidths of TA and TO modes along Γ-X are shown in Figs. 3(b) and 3(c), respectively. The linewidth, known as the full width at half maximum of the phonon peak, is inversely related to the phonon scattering rate [37]

$$2\Gamma_{\boldsymbol{q}j} = \tau_{\boldsymbol{q}j}^{-1} \tag{2}$$

where $2\Gamma_{\mathbf{q}j}$ is the phonon linewidth, and $\tau_{\mathbf{q}j}$ is the scattering rate of the jth phonon mode with the wavevector $\mathbf{q}$. Usually, the phonon linewidth continuously broadens as temperature increases, due to the increase of phonon occupation at high

temperature [21]. Interestingly, as displayed in Figs. 3(b) and 3(c), the linewidths of TA and TO modes at 20 K are both broader than that of phonons at 150 K from zone center to zone boundary, indicating the low temperature anharmonicity in CsI. This is similar to the low temperature anharmonicity in CsCl discovered recently by high resolution x-ray diffraction [26].

The Grüneisen parameter (γ) is a quantity describing the anharmonic interactions of a crystal [38,39]. The mode Grüneisen parameter is defined by the phonon frequency shift with respect to the volume [40]

$$\gamma_j(\boldsymbol{q}) = -\frac{V_0}{\omega_j(\boldsymbol{q})} \frac{\partial \omega_j(\boldsymbol{q})}{\partial V} \tag{3}$$

where V_0 is the equilibrium volume, $\omega_j(\mathbf{q})$ is the phonon energy of wavevector $\mathbf{q}$ and branch index j. We calculated the phonon dispersions with the volumes 1% larger and smaller than the equilibrium volume and extract the Grüneisen parameters from the PHONOPY code [32]. The mode Grüneisen parameters of each mode along Γ-X are shown in Fig. 4(a). It can be seen that the Grüneisen parameters of the transverse modes are larger than those of the longitudinal modes. For example, the γ of TA is two times larger than that of LA
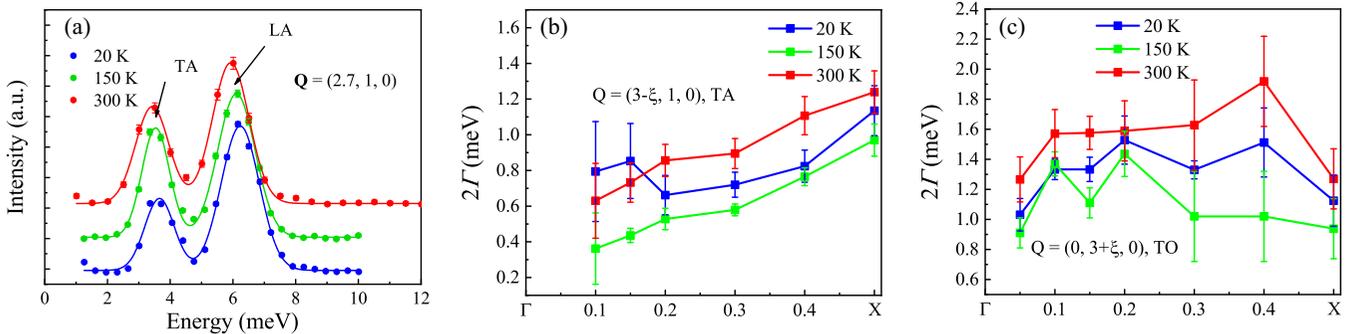
FIG. 3. (a) Phonon lineshapes of CsI at $\mathbf{Q} = (2.7, 1, 0)$ at different temperatures from INS. The error bars are from counting statistics. (b) Phonon linewidth (2Γ) of TA mode. (c) Phonon linewidth (2Γ) of TO mode.
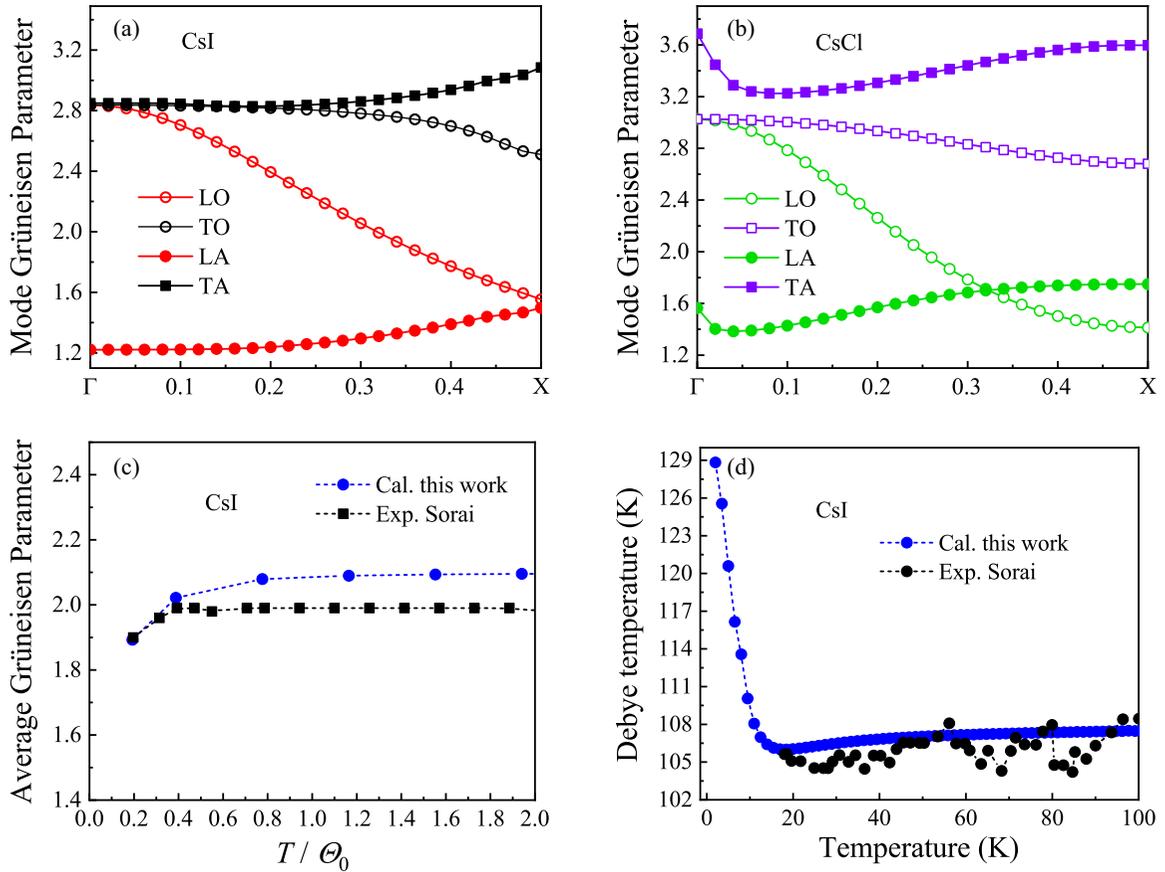
FIG. 4. (a) The mode Grüneisen parameters of CsI along Γ-X. (b) The mode Grüneisen parameters of CsCl along Γ-X. (c) The temperature dependence of the total Grüneisen parameters, the experimental result [41] is also shown for the comparison. (d) The Debye characteristic temperature of CsI. $\Theta_0 = 129.6$ K.

mode from Γ to X, and γ of TO is about twice larger than that of LO mode at the zone boundary. This indicates that the transverse modes (TA and TO) show stronger anharmonicity than the longitudinal modes (LA and LO) in CsI.

Temperature dependence of the average Grüneisen parameters and the Debye characteristic temperature are shown in Figs. 4(c) and 4(d), respectively. It can be clearly seen that γ agrees well with the previous experimental results [44,42]. The large γ confirms the strong anharmonicity in CsI, as reflected through the large linewidth at low temperature from the INS measurement. The large Grüneisen parameters at low temperature were proposed to be related to the isotropy of the elastic constants of the B2-type structure, i.e., the small anisotropy of the shear moduli will not heavily weight the γ value in the B2-type structure (P$m\bar{3}m$) at low temperature

[43]. Therefore, we extracted the group velocities of CsI from the slopes of both the measured acoustic phonon branches by linearly fitting the data around Γ within q $\leqslant 0.2$ and calculated the elastic constants, as shown in Table I. It can be seen that the ratio of elastic module $\frac{1}{2}(C_{11} - C_{12})/C_{44}$ of CsI is indeed close to 1, indicating that the anisotropy of elasticity in CsI is quite small. CsCl was recently discovered to show large low temperature anharmonicity [26]. Therefore, we also calculated its mode Grüneisen parameters along Γ-X, as shown in Fig. 4(b). The mode Grüneisen parameters of TA and TO modes are quite large, confirming its low temperature anharmonicity in CsCl. Different techniques show low temperature anharmonicity in CsI and CsCl, so we conclude that this anharmonicity may exist in all cesium halides compounds.

TABLE I. Elastic constants of CsI (in GPa). The elastic constants of 4.2 K are from previous experimental results [44].

	CsI (DFT, this work)	CsI (4.2 K[a])	CsI (20 K, this work)	CsI (300 K, this work)
C_{11}	28.57	27.25	25.31	20.247
C_{12}	9.62	7.67	6.88	5.861
C_{44}	9.65	8.73	7.65	5.562
$\frac{1}{2}(C_{11} - C_{12})/C_{44}$	0.98	1.12	1.20	1.25

[a]Reference [44].
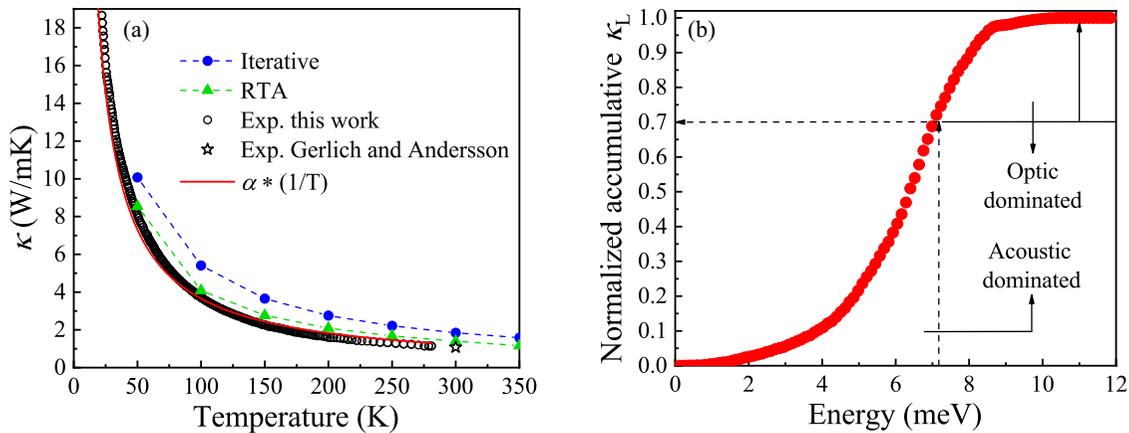
FIG. 5. (a) Temperature dependence of the thermal conductivity of CsI, compared with Gerlich and Andersson's result [5]. Blue circles: our calculation results from iterative solution of BTE; Green triangles: our results from RTA. (b) Normalized accumulative lattice thermal conductivity (at 300 K) with respect to the phonon energy.

B. The low thermal conductivity

The temperature dependence of thermal conductivity of CsI was measured and compared with previous results, as shown in Fig. 5(a). It can be seen that our experimental results are in good agreement with the previous report by Gerlich *et al.* at room temperature [5], and our first-principles results are slightly higher than the experimental values because the phonon scattering of boundaries and defects were not considered in our calculations. We found that the fitting data with $1/T$ function agrees well with our thermal conductivity data, indicating the phonon-phonon Umklapp scattering is the dominant process in CsI at high temperature [45]. This is also reflected by the relaxation time approximation (RTA) values, which take into account normal scattering processes when blocking the heat transport [46]. The thermal conductivity at room temperature is 1.08 W/mK, which is small for such ionic crystals. In addition, the contributions to the normalized accumulative thermal conductivity were also obtained from the first-principles calculations, as shown in Fig. 5(b). Our results indicate that the acoustic phonons dominate the lattice thermal conductivity in CsI, accounting for roughly 70%, while the rest originates from the optic modes. The large contribution from the optic modes is attributed to the unity mass ratio of Cs and I (132.9 vs 126.9), which narrows the acoustic-optic phonon gap and provides a large scattering space for the optic modes.

To investigate the microscopic mechanism of this low thermal conductivity, we focus on the lattice thermal conductivity since the contributions from the electrons can be neglected in the ionic crystal. The lattice thermal conductivity is given by

$$\kappa_{\text{lat}} = \frac{1}{3} \sum_{\mathbf{q}j} c_{\mathbf{q}j} v_{\mathbf{q}j}^2 \tau_{\mathbf{q}j} \tag{4}$$

where $c_{\mathbf{q}j}$ is the heat capacity, $v_{\mathbf{q}j}$ the group velocity, and $\tau_{\mathbf{q}j}$ is the scattering rate of the phonon mode of wave vector $\mathbf{q}$ and branch index j. First, we investigated the group velocities of CsI, which were determined from the slopes of both the calculated and measured acoustic phonon branches by linearly fitting the data around Γ within $q \leqslant 0.2$, as shown in Table II. It can be seen that the group velocities are relatively small

and comparable to the well-known low thermal conductivity materials, such as SnSe and BiCuSeO in which the highest group velocity is 4111 m/s. [21,47]. This indicates that the small group velocity could be one of the primary reasons for the low thermal conductivity of CsI. From 20 to 300 K, the TA velocities decrease by 12.5% and 18% along [100] and [110], respectively, and LA velocities decrease by 10.6% and 8% along [100] and [110], respectively. The group velocities softening results from the thermal effect, which weakens the chemical bonding and further suppresses the thermal conductivity in CsI from 20 to 300 K.

Second, the phonon relaxation time (i.e., phonon scattering rate) is also discussed. Considering the anharmonic IFCs, the phonon scattering rates with absorption and emission processes including each mode were obtained, as shown in Figs. 6(a) and 6(b). As can be seen from the spectra, the scattering rates are smaller than the INS experimental linewidth values (Fig. 3), due to the presence of other scattering processes in the real system, such as boundary, impurities, defects, residual isotopic disorder, and other phonon coupling mechanisms. Besides, the scattering rates possess broad energy range in the low energy region, which is caused by the large number of acoustic modes involved in the three-phonon absorption processes. The acoustic (*a*) phonon branches dominate the phonon absorption processes, known as (*a*, *a*, *a*)

TABLE II. Group velocity of acoustic phonons along the high symmetry directions from INS experimental data and DFT results. (unit in m/s, LA for [100] and [110] directions, TA$_1$ for [100] and [110] directions)

Direction	T (K)	LA	TA
[100]	DFT	2576	1456
	20	2703	1487
	150	2446	1350
	300	2418	1301
[110]	DFT	2365	1613
	20	2216	1788
	300	2044	1466
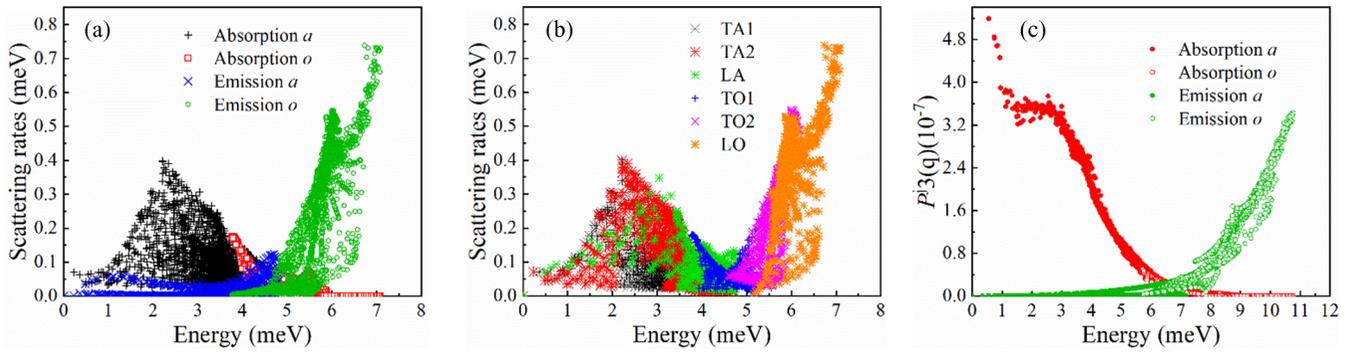
FIG. 6. (a) Scattering rates of CsI at 300 K, including phonon absorption and emission processes. (b) Total scattering rates of each mode at 300 K. (c) Dimensionless phonon scattering phase space volume available for absorption and emission three-phonon scattering processes at 300 K.

processes, and the optic (*o*) phonon branches dominate the emission processes, known as (*a*, *a*, *o*) processes. Since the heat is carried primarily by the acoustic phonons, their scattering by the optic phonons contributes significantly to low thermal conductivity.

We also calculated the dimensionless scattering phase space volume (P_3), as shown in Fig. 6(c). It can be seen that the absorption and emission processes both have large scattering phase space, leading to a short relaxation time for the low thermal conductivity in CsI. The decrease of the phase space volume from absorption to emission processes represents the (*a*, *a*, *a*) processes transferring to (*a*, *a*, *o*) processes. This originates from the mixture of acoustic and optic modes as phonon energy increases, which can also be seen from Fig. 2. This mixture behavior, showing the optic modes overlapped with the acoustic modes in the phonon dispersions, originates from the unity mass ratio of Cs and I that depresses the optic modes. Therefore, the (*a*, *a*, *o*) processes are enhanced and suppress the thermal conductivity of CsI through the combination with the (*a*, *a*, *a*) processes. The (*o*, *o*, *o*) processes are forbidden by the energy conservation condition, while the (*a*, *o*, *o*) processes are severely limited due to the restriction by the conservation of momentum and energy. The total phase space P_3 has a strong negative correlation with thermal conductivity. The total phase space P_3 of CsI is comparable to the well-known low thermal conductivity materials SnSe [48], as shown in Table III. It indicates that the large anharmonic phonon scattering phase space suppresses the thermal conductivity to as low as 1 W/mK in CsI.

By combining with the group velocity and the phonon scattering mechanism, we can conclude that the low

thermal conductivity of CsI is mainly dominated by the acoustic phonons, and the optic phonons play a non-negligible role in the scattering processes. The large phonon scattering rates, strong phonon anharmonicity, and low phonon group velocities jointly lead to the low thermal conductivity of CsI.

IV. CONCLUSIONS

In summary, we investigated the lattice dynamics of CsI by performing the INS, the thermal transport measurements, and the first-principles calculations. The temperature dependent phonon dispersions were obtained and the low temperature anharmonicity was observed from INS measurements. The anharmonicity of transverse optic and acoustic modes were confirmed through the large phonon linewidth and Grüneisen parameters at low temperature. The temperature dependent thermal conductivities were obtained by the thermal transport measurements and the BTE calculations, showing strong phonon-phonon Umklapp scattering at room temperature. Our results revealed that the low thermal conductivity of simple structured CsI originates from the low phonon group velocities and the large anharmonic phonon scattering rates that are dominated by the (*a*, *a*, *a*) and (*a*, *a*, *o*) phonon scattering processes. These results provide a microscopic phonon thermal transport mechanism of CsI, and could also be extended to other cesium halides (e.g., CsCl, CsBr). Our work not only reports the unusual low temperature anharmonicity in CsI, but also reveals the microscopic mechanism of low thermal conductivity in simple structured materials.

TABLE III. The three-phonon scattering phase space of different materials and the related thermal conductivity.

	$P_3(10^{-2}\,\mathrm{eV}^{-1})$	$\kappa_{\exp}$, 300 K (W/mK)
CsI	1.3	1.08[a]
CsCl	1.2[b]	1.14[a]
SnSe	1.9[c]	0.54[c]

[a]Reference [5].
[b]Reference [4].
[c]Reference [48].

[1] S. Bingol, B. Erdinc, and H. Akkus, Int. J. Simul. Multisci. Des. Optim. **6**, A7 (2015).

[2] M. P. Prange, L. W. Campbell, and S. Kerisit, Phys. Rev. B **96**, 104307 (2017).

[3] M. P. Prange, L. W. Campbell, D. Wu, F. Gao, and S. Kerisit, Phys. Rev. B **91**, 104305 (2015).

[4] C. He, C. E. Hu, T. Zhang, Y. Y. Qi, and X. R. Chen, Solid State Commun. **254**, 31 (2017).

[5] D. Gerlich and P. Andersson, J. Phys. C: Solid State Phys. **15**, 5211 (1982).

[6] S. Delpecha, C. Cabetb, C. Slima, and G.S. Picarda, Mater. Today **13**, 34 (2010).

[7] P. Ying, X. Li, Y. Wang, J. Yang, C. Fu, W. Zhang, X. Zhao, and T. Zhu, Adv. Funct. Mater. **27**, 1604145 (2017).

[8] L. M. Daniels, S. N. Savvin, M. J. Pitcher, M. S. Dyer, J. B. Claridge, S. Ling, B. Slater, F. Corà, J. Alaria, and M. J. Rosseinsky, Energy Environ. Sci. **10**, 1917 (2017).

[9] E. S. Toberer, C. A. Cox, S. R. Brown, T. Ikeda, A. F. May, S. M. Kauzlarich, and G. J. Snyder. Adv. Funct. Mater. **18**, 2795 (2008).

[10] E. S. Toberer, A. Zevalkink, and G. J. Snyder, J. Mater. Chem. **21**, 15843 (2011).

[11] P. Andersson, J. Phys. C: Solid State Phys. **18**, 3943 (1985).

[12] G. A. Slack and R. G. Ross, J. Phys. C: Solid State Phys. **18**, 3957 (1985).

[13] S. Pettersson, J. Phys. C: Solid State Phys. **20**, 1047 (1987).

[14] S. Pettersson, J. Phys.: Condens. Matter **1**, 361 (1989).

[15] J. F. Vetelino, K. V. Namjoshi, and S. S. Mitra, Phys. Rev. B **7**, 4001 (1973).

[16] D. N. Payton, M. Rich, and W. M. Visscher, Phys. Rev. **160**, 706 (1967).

[17] M. V. Smirnov, V. A. Khokhlov, and E. S. Filatov, Electrochim. Acta **32**, 1019 (1987).

[18] C. T. Walker, Phys. Rev. **132**, 1963 (1963).

[19] G. Deng, S. Danilkin, H. Zhang, P. Imperia, X. Li, X. Zhao, and H. Luo, Phys. Rev. B **90**, 134104 (2014).

[20] D. Bansal, J. L. Niedziela, R. Sinclair, V. O. Garlea, D. L. Abernathy, S. Chi, Y. Ren, H. Zhou, and O. Delaire, Nat. Commun. **9**, 15 (2018).

[21] C. W. Li, J. Hong, A. F. May, D. Bansal, S. Chi, T. Hong, G. Ehlers, and O. Delaire, Nat. Phys. **11**, 1063 (2015).

[22] Y. Bang, Phys. Rev. B **79**, 054529 (2009).

[23] D. J. Late, S. N. Shirodkar, U. V. Waghmare, V. P. Dravid, and C. N. Rao, Chem. Phys. Chem. **15**, 1592 (2014).

[24] S. Christensen, N. Bindzus, M. Sist, M. Takata, and B. B. Iversen, Phys. Chem. Chem. Phys. **18**, 15874 (2016).

[25] M. Sist, E. M. J. Hedegaard, S. Christensen, N. Bindzus, K. F. F. Fischer, H. Kasai, K. Sugimoto, and B. B. Iversen, IUCrJ **3**, 377 (2016).

[26] M. Sist, K. F. Fischer, H. Kasai, and B. B. Iversen, Angew. Chem. Int. Ed. Engl. **56**, 3625 (2017).

[27] E. D. Bourret-Courchesne, G. A. Bizarri, R. Borade, G. Gundiah, E. C. Samulon, Z. Yan, and S. E. Derenzo, J. Cryst. Growth **352**, 78 (2012).

[28] A. Zheludev, *ResLib 3.4 software* (Oak Ridge National Laboratory, Oak Ridge, Tennessee 2007); http://www.neutron.ethz.ch/research/resources/reslib.

[29] S. W. Lovesey, *The Theory of Neutron Scattering from Condensed Matter* (Oxford University Press, Oxford, 1985), pp. 296–303 .

[30] Z. Y. Zhao, X. M. Wang, C. Fan, W. Tao, X. G. Liu, W. P. Ke, F. B. Zhang, X. Zhao, and X. F. Sun, Phys. Rev. B **83**, 014414 (2011).

[31] G. Kresse and J. Furthmüller, Phys. Rev. B **54**, 11169 (1996); Comput. Mater. Sci. **6**, 15 (1996).

[32] A. Togo, F. Oba, and I. Tanaka, Phys. Rev. B **78**, 134106 (2008).

[33] W. Li, J. Carrete, N. A. Katcho, and N. Mingo, Comput. Phys. Commun. **185**, 1747 (2014).

[34] S. Mukhopadhyay, D. Bansal, O. Delaire, D. Perrodin, E. Bourret-Courchesne, D. J. Singh, and L. Lindsay, Phys. Rev. B **96**, 100301(R) (2017).

[35] C. M. Foster, M. Grimsditch, Z. Li, and V. G. Karpov, Phys. Rev. Lett. **71**, 1258 (1993).

[36] C. D. O'Neill, D. A. Sokolov, A. Hermann, A. Bossak, C. Stock, and A. D. Huxley, Phys. Rev. B **95**, 144101 (2017).

[37] R. A. Cowley, Rep. Prog. Phys. **31**, 123 (1968).

[38] D. L. Nika and A. A. Balandin, J. Phys.: Condens. Matter **24**, 233203 (2012).

[39] J. P. Heremans, Nat. Phys. **11**, 990 (2015).

[40] K. Brugger, Phys. Rev. **137**, A1826 (1965).

[41] M. Sorai, J. Phys. Soc. Jpn. **25**, 421 (1968).

[42] S. Ganesan and R. Srinivasan, Proc. R. Soc. A **271**, 154 (1963).

[43] G. K. White, Proc. R. Soc. Lond. A **286**, 204 (1965).

[44] B. J. Marshall and J. R. Kunkel, J. Appl. Phys. **40**, 5191 (1969).

[45] T. M. Tritt, *Thermal Conductivity: Theory, Properties, and Applications* (Kluwer Academic / Plenum, New York, 2004).

[46] A. Ward, D. A. Broido, D. A. Stewart, and G. Deinzer, Phys. Rev. B **80**, 125203 (2009).

[47] Y. L. Pei, J. He, J. F. Li, F. Li, Q. Liu, W. Pan, C. Barreteau, D. Berardan, Nita Dragoe, and L. D. Zhao, NPG Asia Mater. **5**, e47 (2013).

[48] J. Carrete, N. Mingo, and S. Curtarolo, Appl. Phys. Lett. **105**, 101907 (2014).